

A conjugate study of mean winds and planetary waves employing enhanced meteor radars at Rio Grande, Argentina (53.8°S) and Juliusruh, Germany (54.6°N)

D. C. Fritts,¹ H. Iimura,¹ R. Lieberman,¹ D. Janches,² and W. Singer³

Received 16 June 2011; revised 4 January 2012; accepted 4 January 2012; published 8 March 2012.

[1] Two meteor radars with enhanced power and sensitivity and located at closely conjugate latitudes (54.6°N and 53.8°S) are employed for interhemispheric comparisons of mean winds and planetary wave structures at periods of ~ 8 to 20 days. Our study uses data from June 2008 through May 2010 during which both radars provided nearly continuous wind measurements from ~ 80 to 100 km. Monthly mean winds at 53.8°S exhibit a stronger westward zonal jet in spring and early summer at lower altitudes and no westward winds at higher altitudes. In contrast, westward mean winds of ~ 5 – 10 ms^{-1} at 54.6°N extend to above 96 km during late winter and early spring each year. Equatorward mean winds extend approximately from spring to fall equinox at both latitudes with amplitudes of ~ 5 – 10 ms^{-1} . Meridional mean winds are more variable at both latitudes during fall and winter, with both poleward and equatorward monthly means indicating longer-period variability. Planetary waves seen in the 2 day mean data are episodic and variable at both sites, exhibit dominant periodicities of ~ 8 – 10 and 16 – 20 days and are more confined to late fall and winter at 54.6°N. At both latitudes, planetary waves in the two period bands coincide closely in time and exhibit similar horizontal velocity covariances that are positive (negative) at 54.6°N (53.8°S) during peak planetary wave responses.

Citation: Fritts, D. C., H. Iimura, R. Lieberman, D. Janches, and W. Singer (2012), A conjugate study of mean winds and planetary waves employing enhanced meteor radars at Rio Grande, Argentina (53.8°S) and Juliusruh, Germany (54.6°N), *J. Geophys. Res.*, 117, D05117, doi:10.1029/2011JD016305.

1. Introduction

[2] Ground-based studies of the mesosphere and lower thermosphere (MLT) have addressed interhemispheric differences in mean temperatures and winds, tides, planetary waves (PWs), gravity waves (GWs), and the constituent distributions and microphysical processes that depend on them from midlatitudes to polar latitudes [e.g., Vincent *et al.*, 1988; Avery *et al.*, 1989; Portnyagin *et al.*, 1993a, 1993b, 2006; Fraser *et al.*, 1995; Huaman and Balsley, 1999; Dowdy *et al.*, 2001, 2007; Chu *et al.*, 2003; Kishore *et al.*, 2003; Riggan *et al.*, 2003; Day and Mitchell, 2010a, 2010b; Iimura *et al.*, 2011]. Similar studies employing satellite data have provided a more uniform global perspective for specific fields. These include mean stratospheric and MLT temperatures, tidal and PW signatures in MLT temperatures, and polar mesospheric cloud (PMC) distributions that depend critically on mesopause temperature and H₂O distributions

[e.g., Andrews, 1989; Siskind *et al.*, 2003; Hervig and Siskind, 2006; Huang *et al.*, 2006; Bailey *et al.*, 2007; Xu *et al.*, 2007a, 2007b; Mukhtarov *et al.*, 2010].

[3] Interhemispheric comparisons of MLT wind fields have been more limited to date. Nevertheless, measurements by HRDI aboard the UARS satellite, TIDI aboard the TIMED satellite, and several meteor and medium-frequency (MF) radars at polar latitudes have revealed interhemispheric asymmetries in mean, tidal, and PW wind fields [e.g., Vial, 1989; Burrage *et al.*, 1995; Oberheide *et al.*, 2006; Day and Mitchell, 2010a, 2010b; Iimura *et al.*, 2010, 2011, and references therein]. Mean zonal winds were seen to be stronger over Syowa Station ($\sim 69^\circ\text{S}$) than over Andenes, Norway ($\sim 69^\circ\text{N}$) by $\sim 10 \text{ ms}^{-1}$ in summer and winter, while mean meridional winds were seen to be stronger over Syowa in summer, but weaker in winter [Iimura *et al.*, 2011]. Larger nonmigrating semidiurnal tides were also seen to occur over the Antarctic than over the Arctic [Iimura *et al.*, 2010]. In contrast, ~ 16 day wave amplitudes and seasonal occurrence were found to be very similar between the Arctic and Antarctic at $\sim 68^\circ\text{N}$ and S [Day and Mitchell, 2010b], though large interannual variability was also noted.

[4] Our purpose in this paper is to employ new capabilities for conjugate interhemispheric MLT wind measurements that recently became available with the installation of a new generation meteor radar at the southern tip of South America. The Southern Argentina Agile Meteor Radar (SAAMER)

¹Colorado Research Associates Division, NorthWest Research Associates, Boulder, Colorado, USA.

²Space Weather Division, NASA Goddard Space Flight Center, Greenbelt, Maryland, USA.

³Leibnitz Institute of Atmospheric Physics, Rostock University, Kühlungsborn, Germany.

began measurements in May 2008 at Rio Grande, Tierra del Fuego (TdF), Argentina (53.8°S, 67.7°W) [Fritts *et al.*, 2010a, hereafter F10]. This radar is closely conjugate in latitude to a similar meteor radar at Juliusruh (JLR), Germany (54.6°N, 13.6°E) [Singer *et al.*, 2003]. Wind measurements with each radar are employed for a conjugate study of the mean winds and PWs having periods from ~ 8 to 20 days measured with the TdF and JLR radars during the 24 months since installation of the TdF radar. Shorter-period PWs will be addressed in a future paper. Descriptions of the radars and our analysis methods are provided in section 2. Sections 3 and 4 present our measurement results and discussion of the monthly mean winds and PW structures, respectively. A discussion of these results and our conclusions are provided in sections 5 and 6.

2. Radar Descriptions and Data Analysis

2.1. Radar Descriptions

[5] As described by F10, SAAMER on TdF was specifically designed to enable high-resolution definition of the large-scale wind field. This is accomplished with a radar frequency and bandwidth of 32.55 and 0.3 MHz, respectively, a peak power of 60 kW, and an eight-antenna transmitting array using three-element crossed Yagis. This configuration directs the majority of radar power into eight beams centered at an off-zenith angle of $\sim 35^\circ$. Five receiver channels enable redundant meteor position definition. A 2-baud, 26- μ s pulse yields a 2 km range resolution that is oversampled by 2 times. The pulse repetition frequency is 2144 Hz. These capabilities yield an average $\sim 16,000$ accepted meteor detections each day (monthly means from $\sim 8,000$ to 24,000) at $<50^\circ$ zenith angles and $\sim 90\%$ of these occurring between altitudes of 80 and 100 km. These meteor detections are easily sufficient to define the mean and PW motions of interest here with high precision. Additional details are provided by F10.

[6] The JLR meteor radar employed for this study is identical to the one observing until August 2001 [Singer *et al.*, 2003, 2004a, 2004b, 2005; Szasz *et al.*, 2004]. The radar operates at a frequency of 32.55 MHz with a peak power of 15 kW, a pulse length of 13.3 μ s, and a pulse repetition frequency of 2144 Hz. The system utilizes a three-element Yagi antenna for transmission and a five-antenna interferometer for reception. This antenna configuration determines a meteor location with resolutions of 2 km in range and 2° in angle. Daily count rates vary between $\sim 6,000$ and $\sim 13,000$ accepted meteors throughout the year. These meteor counts are sufficiently high to have confidence in the radar determination of mean and PW winds.

2.2. Data Analysis

[7] Hourly mean zonal and meridional winds were determined by fitting a mean horizontal wind in each 3 km altitude bin centered from 81 to 99 km for each hour of meteor radial velocity measurements at off-zenith angles between 15° and 50° . These estimates included ~ 120 meteors/h at 90 km on average, and a minimum count of 5 meteors/h was required for a valid horizontal wind estimate. Daily and 2 day mean zonal and meridional winds were then computed for each day if a minimum of 12 and 36 hourly wind estimates were available, respectively. Daily means effectively remove tidal

motions while 2 day means minimize contributions from the quasi 2 day wave (2DW) and reduce contributions by the 5 day wave. Missing daily or 2 day means were interpolated from third-order spline fits.

[8] PW contributions to the motion field were identified and analyzed in several ways. An S transform analysis [Stockwell *et al.*, 1996] was performed to reveal the annual variations of the dominant PW periods at each site. For our purposes here, the S transform employed a Gaussian full-width half maximum equal to the period evaluated. Given the dominant periods observed, the structure and variability of these motions are examined in greater detail by employing band-pass filters spanning periods of 7–12 and 12–24 days [Isoda *et al.*, 2002; Murphy *et al.*, 2007]. Band pass winds were also employed to compute PW wind hodographs, variances, and horizontal momentum fluxes to aid the interpretation of these motions. Our analyses employing these results are discussed in detail below.

[9] We note that the two radars, while nearly conjugate in latitude, are separated by $\sim 80^\circ$ of longitude. Thus, we might expect some differences in mean winds, given the location of SAAMER in a global “hotspot” of GW activity that can impact MLT mean winds locally [Fritts *et al.*, 2010b]. We do not expect significant variations in traveling PW climatologies in longitude, apart from possible secondary influences of longitudinally varying mean winds. However, both mean and PW winds could be impacted by the presence and variations of quasi-stationary PWs which radars at single sites cannot characterize.

3. Mean Winds

[10] Zonal and meridional winds from 81 to 96 km averaged for 2 and 30 days are shown in Figures 1 and 2, respectively. Winds over JLR are shown in Figures 1a, 1b, 2a, and 2b and winds over TdF are shown in Figures 1c, 1d, 2c, and 2d. The 2 day mean winds exhibit variability on time scales of ~ 5 to 30 days about the 30 day mean winds suggestive of PW and lower-frequency motions having amplitudes comparable to or exceeding the 30 day mean winds throughout the annual cycle, particularly over TdF. Here we focus on the seasonal behavior of the 30 day mean winds. PW variability will be addressed in section 4.

[11] The 30 day mean winds shown in Figure 2 reveal significant qualitative and quantitative differences between the two sites. Considering first the zonal mean winds (Figures 2a and 2c), we see that westward mean winds over JLR descend from the highest altitudes beginning ~ 1 month before spring equinox and reach an altitude of ~ 81 km approximately a month later. They persist for ~ 1 –2 months above ~ 88 km and for ~ 4 –5 months below and have maximum 30 day westward winds of $\sim 25 \text{ ms}^{-1}$. In contrast, summer 30 day westward winds over TdF do not descend from above, but appear first at lower altitudes ~ 1 month after spring equinox. They reach altitudes of ~ 90 km within ~ 2 –4 weeks and occur only briefly above ~ 88 km (~ 1 month or less), but persist at lower altitudes for ~ 3 –4 months. 30 day westward winds are also ~ 10 – 20 ms^{-1} stronger during spring 2008 over TdF than observed either year over JLR, achieving a maximum exceeding 40 ms^{-1} during November and December 2008.

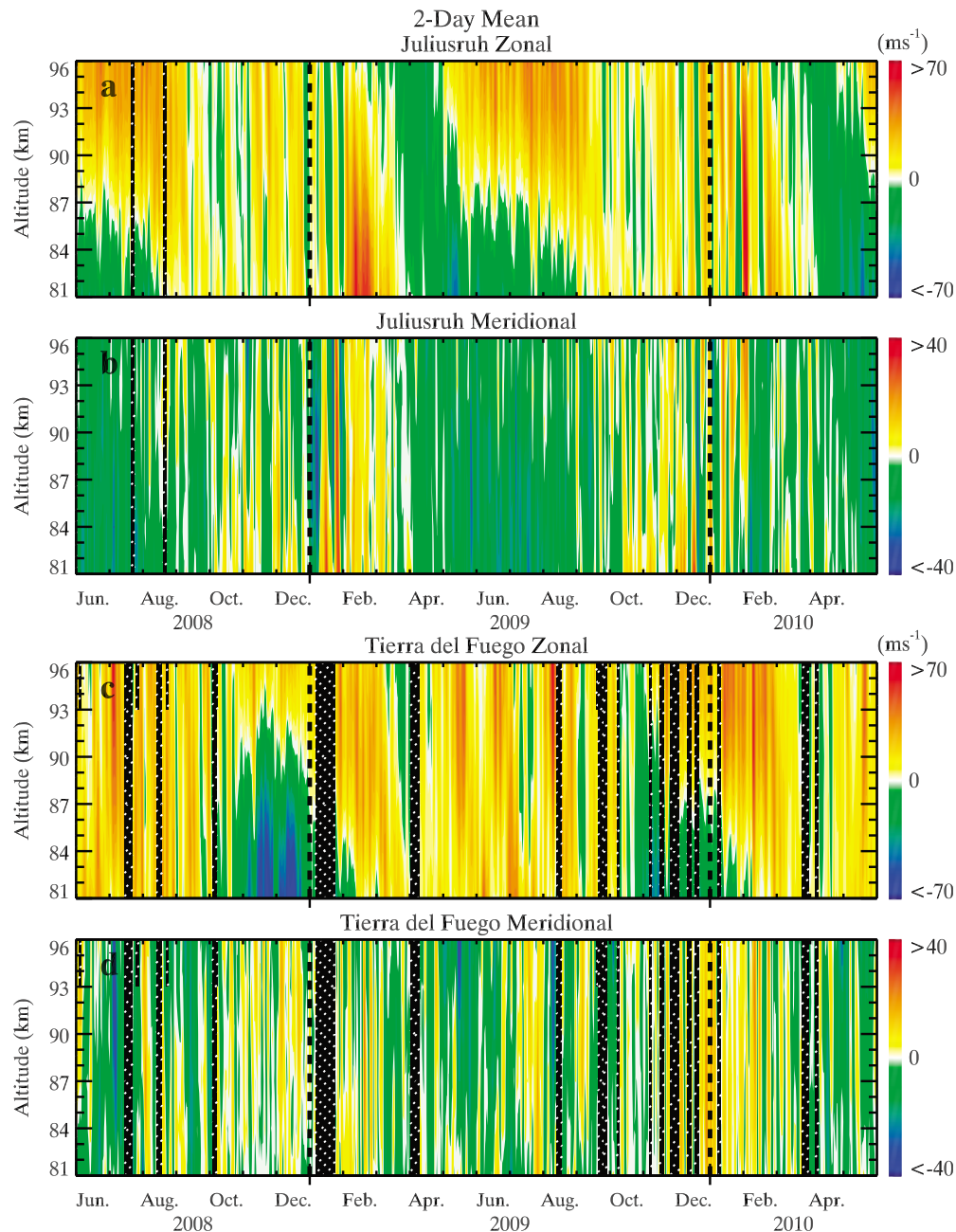


Figure 1. Time-height displays of 2 day mean (a and c) zonal and (b and d) meridional winds over JLR (Figures 1a and 1b) and TdF (Figures 1c and 1d) from June 2008 through May 2010. Hatched regions indicate missing or insufficient data to provide mean or PW wind estimates.

[12] Summer 30 day mean eastward winds over JLR appear at the highest altitudes ~ 1 month after spring equinox and descend quickly to $\sim 85\text{--}88$ km, but not to the lowest altitudes until $\sim 1\text{--}2$ months after summer solstice. Unlike mean zonal winds over JLR, eastward 30 day mean winds prevail throughout the year above ~ 92 km over TdF. Onsets of summer 30 day eastward winds at higher altitudes over TdF are less well defined, because there are not early spring 30 day westward mean winds at higher altitudes and PW influences on 2 day mean winds are much larger than over JLR (see Figure 1). Nevertheless, they appear to occur $\sim 1\text{--}2$ months after spring equinox (see the apparently later

transition in 2008 than in 2009) and to descend somewhat more quickly to the lowest altitudes over TdF than over JLR. Magnitudes are similar between sites, and there is discernable but slow variability in the 30 day means at the higher altitudes at each site having a periodicity of ~ 100 days.

[13] Eastward 30 day mean winds extend from ~ 1 month before fall equinox to after spring equinox throughout the altitude interval measured over JLR, and are even more extended in time over TdF. These fall and winter eastward mean winds are more variable in time at each site than during spring and summer, with apparent periodicities of $\sim 60\text{--}90$ days. Also seen is a reduction in eastward mean winds

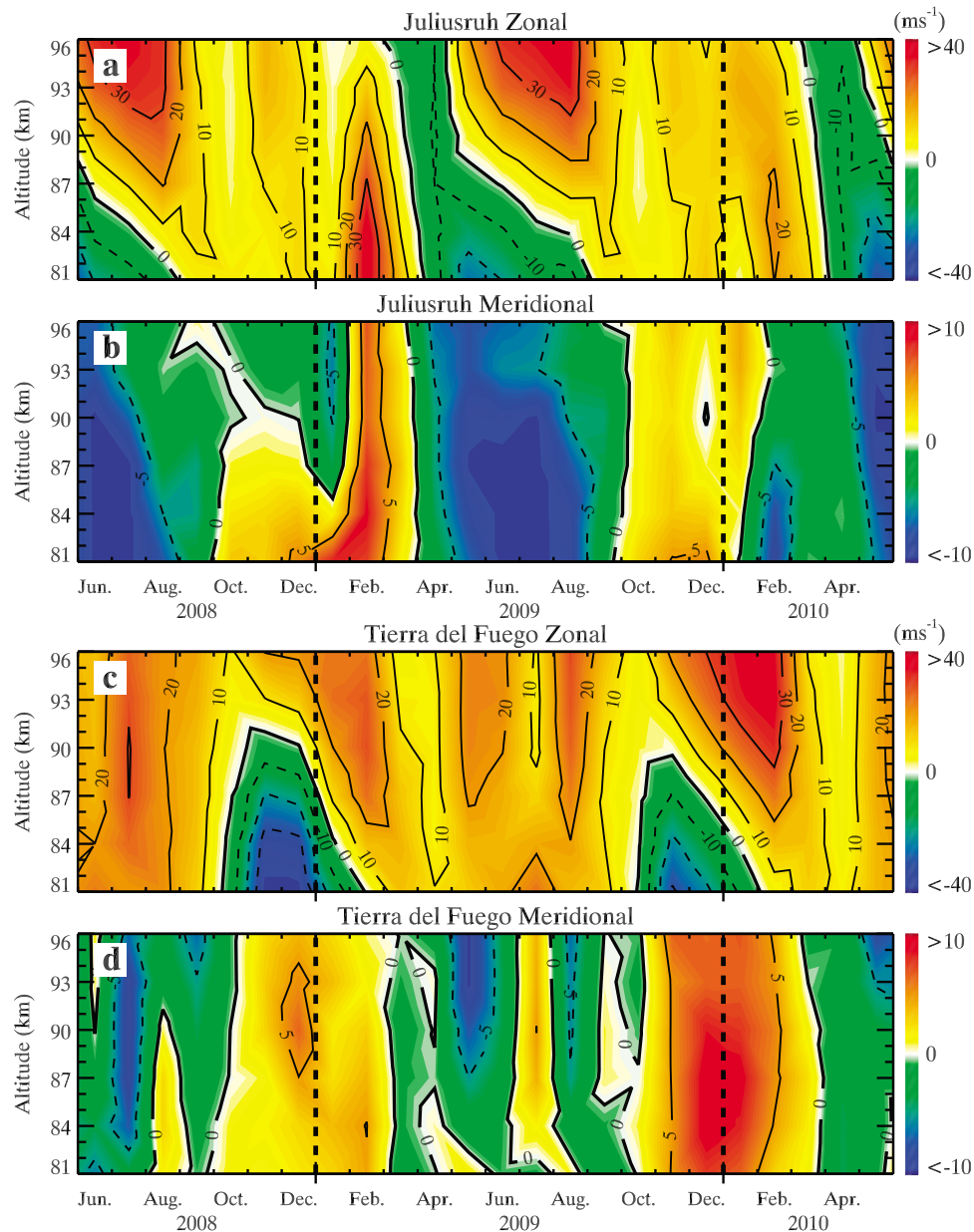


Figure 2. As in Figure 1 but for 30 day means at 5 day intervals.

over JLR during January 2009 at higher altitudes and a corresponding strong enhancement during February 2009 accompanying the strongest and most persistent sudden stratospheric warming ever observed [Manney *et al.*, 2009].

[14] The onset of persistent equatorward 30 day mean winds (see Figures 2b and 2d) is highly variable over both sites, varying from as much as ~ 2 months before to ~ 1 month after spring equinox during our observation period. 30 day mean equatorward winds persist for ~ 5 – 6 months over both sites, with the onset and cessation over each site apparently strongly influenced by PW activity extending from \sim fall to spring equinox. 30 day mean equatorward winds exceed 10 ms^{-1} below ~ 90 km near summer solstice over JLR, but are somewhat weaker and extend to higher altitudes near summer solstice over TdF. The 30 day mean meridional winds from fall to spring equinoxes are seen

to be much more variable over both sites. Seasonal means are poleward and weak, but 30 day means are poleward and equatorward over both sites, and there is greater apparent variability over TdF.

4. Planetary Waves

4.1. S Transforms

[15] A more quantitative perspective on zonal and meridional wind variability on PW time scales is provided in Figure 3 with S transforms of the 2 day mean winds at 84 and 96 km (left and right) over JLR and TdF (top and bottom). These exhibit significant differences between the two altitudes at each site. Strong seasonal responses are seen simultaneously at 84 and 96 km in a number of cases, but there are other strong responses at one altitude that are not

significant at the other (especially in the zonal component over TdF). Also seen is a tendency for greater temporal confinement of the strong PW responses over JLR (top panels). Here the strongest responses are seen to extend from slightly before winter solstice into February (~ 2 months after winter solstice). Responses over TdF (bottom panels), in contrast, begin ~ 1 – 2 months before winter solstice, extend ~ 4 months or more beyond winter solstice, especially in the zonal motions and at 96 km, and appear to be more episodic and less coherent among different PW periods. Specific examples of PW responses over JLR include: (1) coherent maxima at 84 and 96 km that are most pronounced in the meridional component beginning in January 2009, appear first at a period of ~ 16 days, and rapidly yield stronger maxima at periods from ~ 8 – 12 days; and (2) a similar event beginning in late November of 2009, again with an initial period of ~ 16 days, but now with maxima in the meridional component at 84 km and in the zonal component at 96 km; a subsequent maximum again extends to periods of ~ 8 – 12 days accompanying the attainment of the strong maximum at ~ 16 days; additional maxima occur at PW periods of ~ 10 and 20 days (in the meridional and zonal components, respectively) ~ 1 – 2 months later, suggesting a coupling of modes and/or evolution of the maximum response to shorter periods based on the zonal behavior at 96 km.

[16] Corresponding PW or longer-period responses over TdF include: (3) a relatively discrete maximum at 96 km at an initial period of ~ 16 days in the meridional component in early June 2008 and rapid successive (and stronger) maxima in the zonal component at periods of ~ 8 – 10 , 20, and 40 days quickly thereafter; (4) additional isolated maxima from June to August 2008 at a period of ~ 10 days in the meridional component at 84 km and in the zonal component at 96 km, and at a period of ~ 16 days in the meridional response at 96 km; and (5) relatively isolated maxima at periods of ~ 30 – 40 and 16 – 20 days from June–December 2008 and from May–September 2009 seen primarily in the zonal winds at higher altitudes.

[17] Observed PW periods are generally consistent with the normal modes expected from classical theory assuming a stationary, isothermal, and inviscid atmosphere [Volland, 1988; Forbes, 1995]. Normal modes having the gravest zonal wave number $s = 1$ are expected (and observed) to exhibit a range of periods from ~ 5 days to ~ 16 days, with westward phase speeds varying inversely with the period. However, their latitudinal and vertical structures and periods may differ significantly from the idealized modal structures due to the variations of mean winds and temperatures with latitude and altitude [Salby, 1981a, 1981b].

[18] PWs appear in the MLT in number of ways. Evidence suggests that 5 day and 16 day waves arising at lower altitudes in the winter hemisphere propagate directly into the winter MLT, but may also appear in the summer MLT due to propagation from the winter hemisphere at altitudes above the summer mesospheric jet [Forbes et al., 1995; Miyoshi, 1999]. PW westward phase speeds are comparable to westward mean winds in the summer stratosphere and mesosphere, suggesting possibilities for generation or amplification by barotropic, baroclinic, or optimal instabilities as well as PW-mean flow interactions [e.g., Simmons et al., 1978;

Charney and Straus, 1980; Hirooka and Hirota, 1985; Smith, 1985; Randel et al., 1987; Farrell, 1988; Farrell and Ioannou, 1996]. PWs have also been suggested to arise from in situ excitation in the MLT due to differential momentum deposition in the MLT accompanying modulation of GW sources or filtering at lower altitudes [Williams and Avery, 1992; Forbes et al., 1995; Smith, 2003].

[19] While longer-period oscillations are seen in the MLT at equatorial and higher latitudes [e.g., Eckermann et al., 1997; Luo et al., 2001], these are likely not PW normal modes, given the observed phase structures and expectations of strong influences by mean winds at these periods [see Forbes, 1995, and references therein]. Instead, they appear to accompany longer-period oscillations, e.g., the Madden-Julian oscillation [Madden and Julian, 1994], which modulate tropical convection in the troposphere.

[20] Of the various PW modes anticipated by theory, we thus expect the most prominent to be the “10 day” and “16 day” PWs within the frequency band displayed in Figure 3, based on observations at many sites. Our S transform results are consistent with this, and with the expectation of strong wave-wave and wave-mean flow interactions and the rapid temporal variability of the wind fields accompanying these various interactions.

4.2. Band Pass Results

[21] In order to determine which PW periods contribute the dominant zonal and meridional wind responses having continuity in altitude, we examine the S transform results as functions of altitude for periods of 8, 10, 12, 16, 20, 30, and 40 days. The largest and most coherent responses occur at periods of 10, 16, 20, and 40 days, and S transform amplitudes for these periods are shown in Figure 4 as functions of altitude. Examination of these fields reveals the following:

[22] 1. The ~ 10 day oscillations (maxima ~ 15 – 25 ms^{-1}) including (1) over JLR in January 2009 and from December 2009 to February 2010 primarily in the meridional component, (2) over TdF during July and August 2008 at higher and lower altitudes, respectively, (3) over TdF during September and October 2008 at all altitudes, and (4) episodically over a range of altitudes from \sim July 2009 to April 2010;

[23] 2. The ~ 16 day oscillations including (1) over JLR from November 2008 to February 2009 and from November 2009 into February 2010 (with maxima of ~ 10 – 15 ms^{-1}), and (2) over TdF from \sim June to October 2008, from April to September 2009, and episodically from December 2009 to May 2010;

[24] 3. The ~ 20 day oscillations (maxima ~ 8 – 16 ms^{-1}) including (1) over JLR during November 2008 to January 2009, from May to July 2009 at lower altitudes, and from December 2009 to February 2010 (with maxima in the zonal component in each case) and (2) over TdF sporadically from June to December 2008, from May to September 2009, during December 2009 and January 2010, and during April and May 2010; and

[25] 4. The ~ 40 day oscillations (maxima ~ 10 – 12 ms^{-1}) including (1) over JLR from June to August 2008, from December 2008 to March 2009, and from September to December 2009 and (2) over TdF during June and July 2008 and from April to October 2009 (with maxima in the zonal component in each case).

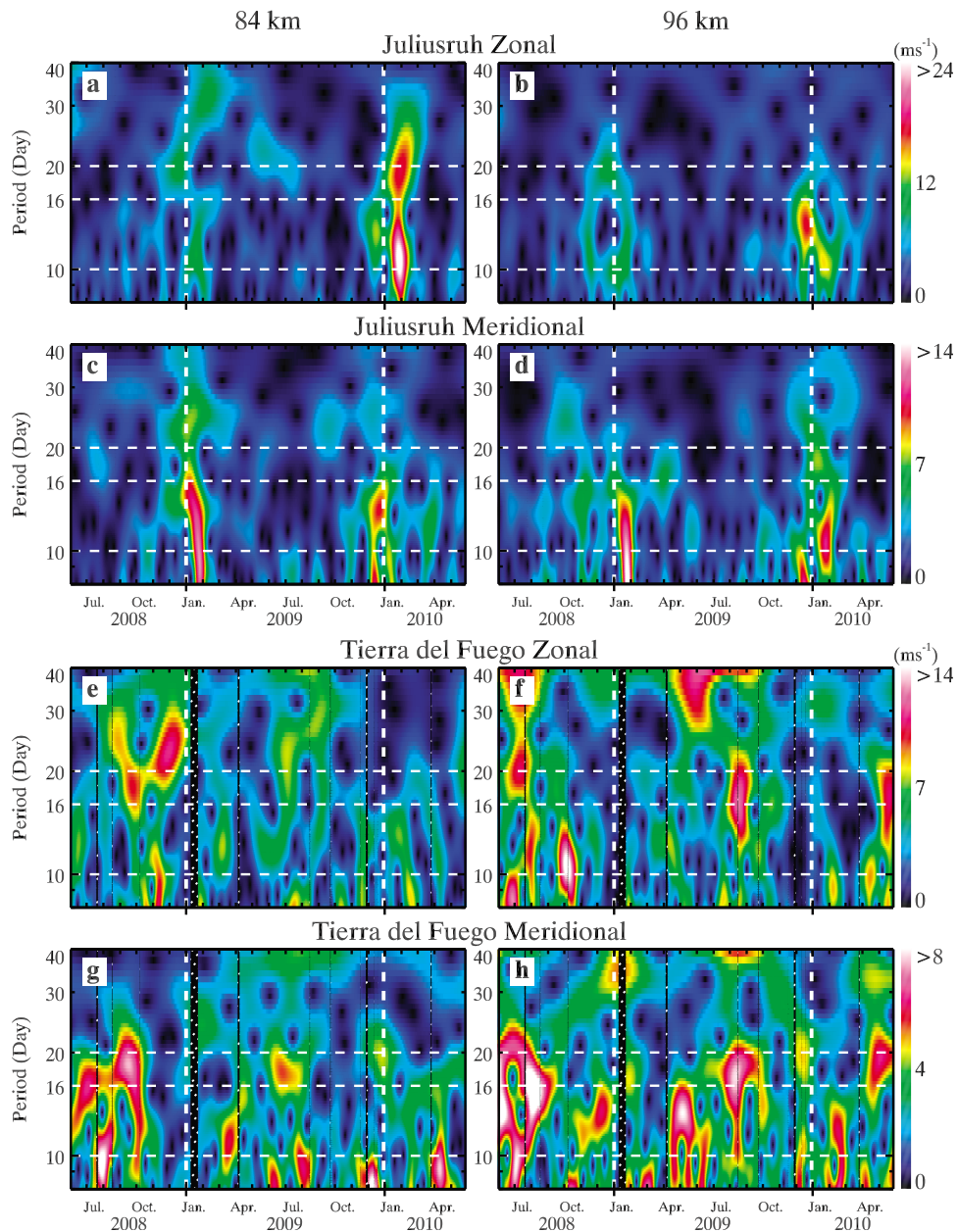


Figure 3. S transforms as functions of time and period of 2 day mean (a, b, e, and f) zonal and (c, d, g, and h) meridional winds at 84 (Figures 3a, 3c, 3e, and 3g) and 96 km (Figures 3b, 3d, 3f, and 3h) for JLR (Figures 3a–3d) and TdF (Figures 3e–3h) from June 2008 through May 2010. Note the clear seasonal variations and consistency between the zonal and meridional motions over JLR, and the lack of clear seasonal variations and consistency between the zonal and meridional motions over TdF. Hatched regions are as in Figure 1.

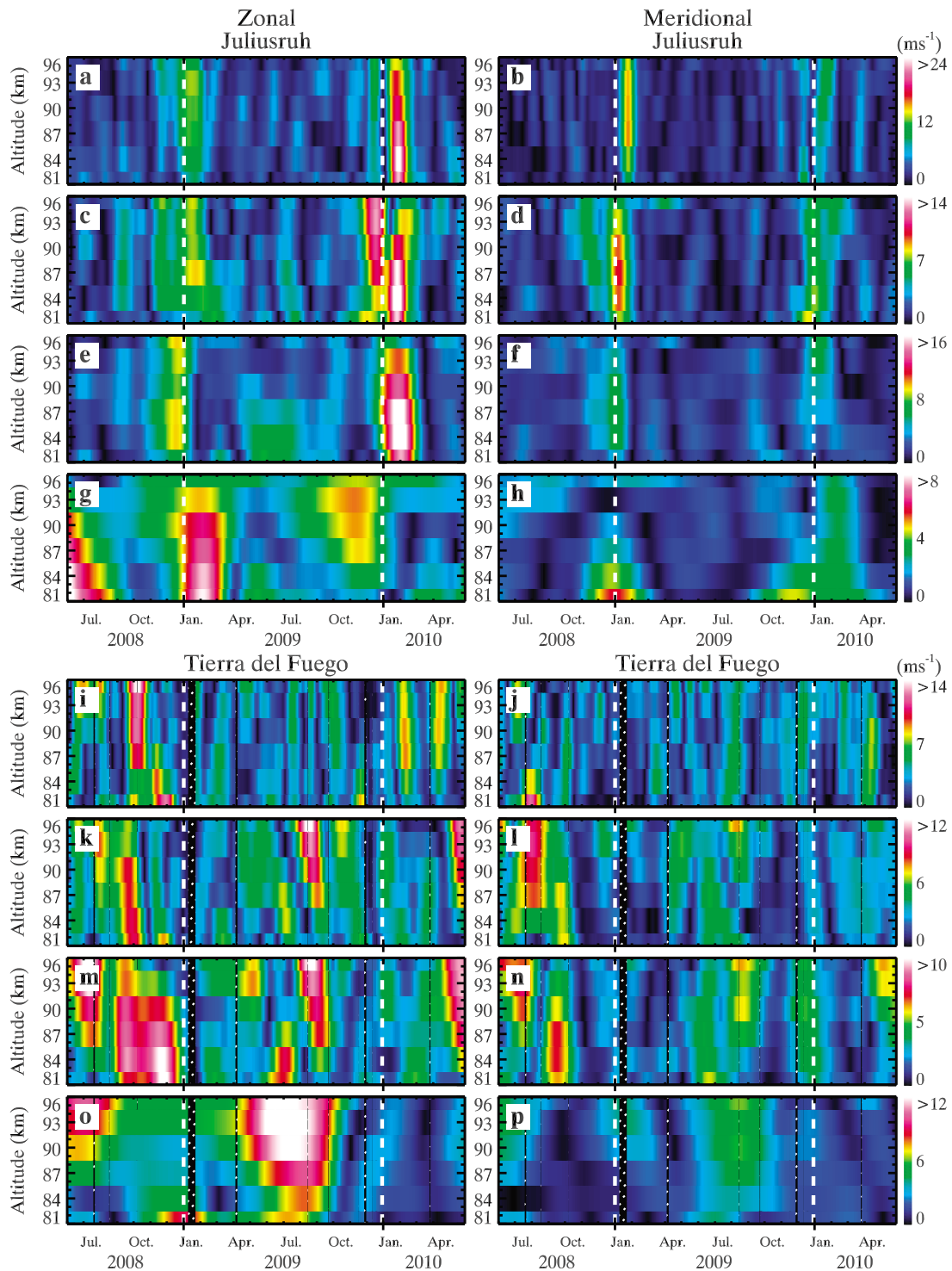


Figure 4. S transform amplitudes as functions of time and altitude for periods of (a, b, i, and j) 10, (c, d, k, and l) 16, (e, f, m, and n) 20, and (g, h, o, and p) 40 days. Figures 4a, 4c, 4e, 4g, 4i, 4k, 4m, and 4o (Figures 4b, 4d, 4f, 4h, 4j, 4l, 4n, and 4p) show the zonal (meridional) components, respectively. Hatched regions are as in Figure 1.

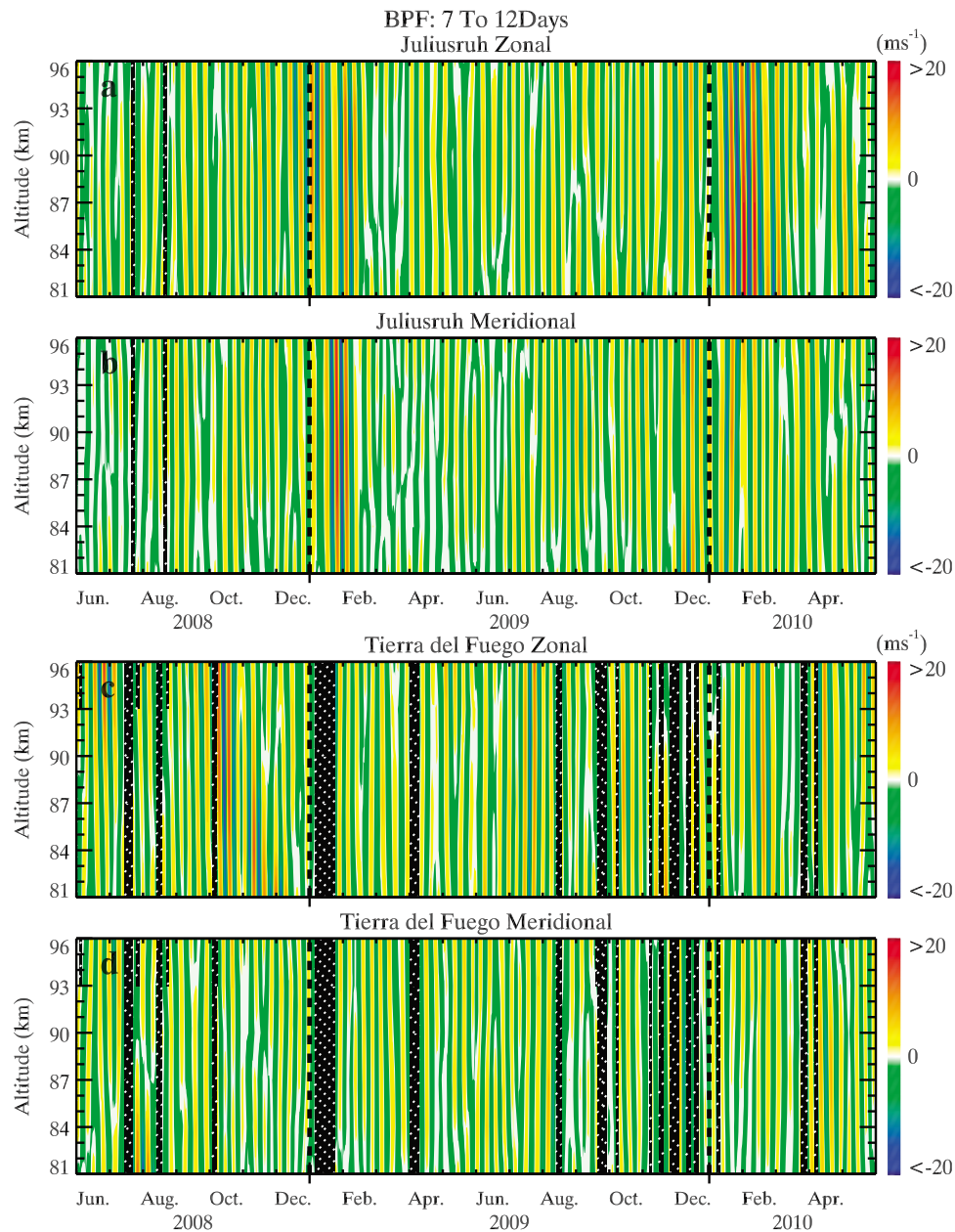


Figure 5. Time-height displays of (a and c) zonal and (b and d) meridional 7–12 day band-pass winds over JLR (Figures 5a and 5b) and TdF (Figures 5c and 5d) from June 2008 through May 2010. Hatched regions are as in Figure 1.

[26] The dominant S transform responses suggest that ~ 8 – 10 day and ~ 16 – 20 day PWs account for the major variability of the MLT wind field. They also reveal that longer-period oscillations make important contributions, as seen clearly in the ~ 30 – 40 day mean wind variations between fall and spring equinoxes in Figure 1 (especially over TdF) and the ~ 90 day variations during the same periods in Figure 2. To examine the amplitudes and phase structures of the motions that are most easily identified as PWs more closely, we display in Figures 5 and 7 contours of the zonal and meridional winds over JLR and TdF (at top and bottom) for 7–12 and 12–24 day band passes. Shown in Figure 6 are the band-passed zonal and meridional amplitudes at 3 km intervals from 81 to 96 km for the 7–12 day

(Figures 6a, 6b, and 6e) and 12–24 day (Figures 6c, 6d, and 6f) band passes over JLR and TdF. These are shown for the fall and winter seasons over JLR, and for the full annual cycle over TdF, to more easily display relative phases and amplitudes within and between these PW bands.

4.2.1. The ~ 8 – 10 Day PWs

[27] Consider first the 7–12 day band pass results shown in Figure 5 (chosen to largely exclude influences of the 6.5 day PW). These show that the ~ 10 day PWs over JLR exhibit distinct late fall to early winter maxima extending over ~ 2 – 3 months during the 2 years studied. These amplitudes are also displayed in Figures 6a–6d at each altitude for the two fall and winter seasons with the wind components overlaid to more easily identify their relative phases. We note that

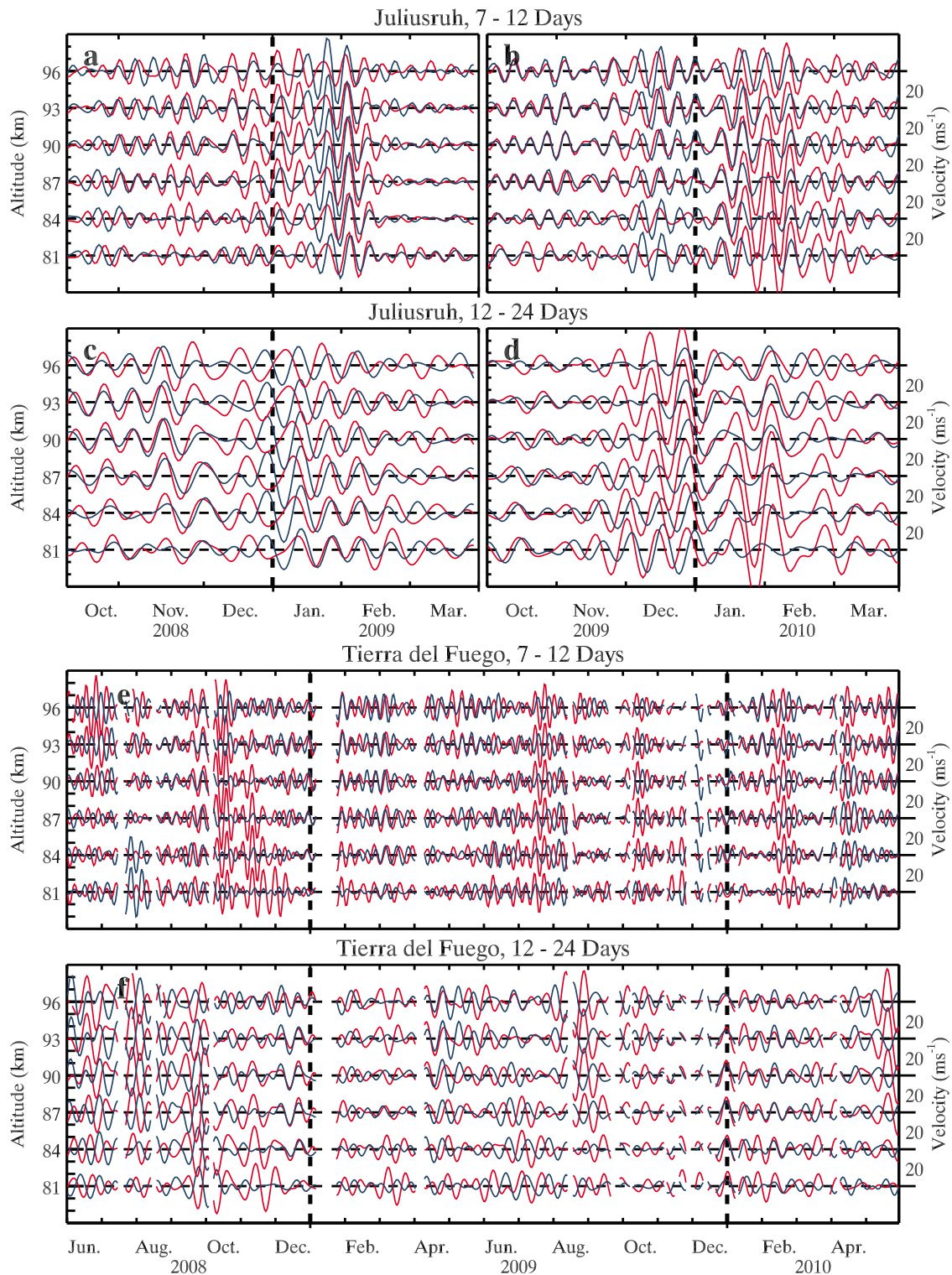


Figure 6. Band pass winds at 3 km intervals from 81 to 96 km over (a–d) JLR and (e and f) TdF. Band passes are 7–12 (Figures 6a, 6b, and 6e) and 12–24 days (Figures 6c, 6 d, and 6f). Intervals are October 2008 to March 2009 (Figures 6a and 6c), October 2009 to March 2010 (Figures 6b and 6 d), and June 2008 to May 2010 (Figures 6e and 6f). Red and blue denote zonal and meridional winds, respectively.

these band-passed amplitudes exhibit both smoothed temporal variability and somewhat smaller maximum amplitudes (now $\sim 20 \text{ ms}^{-1}$) than seen in the S transforms in Figure 3. This is expected for the relatively narrow band passes

necessary to distinguish between closely spaced PW periods examined here. Also seen clearly is the commencement of the major ~ 10 day PW arising in December 2008 earlier in the zonal component. Comparable meridional amplitudes lag

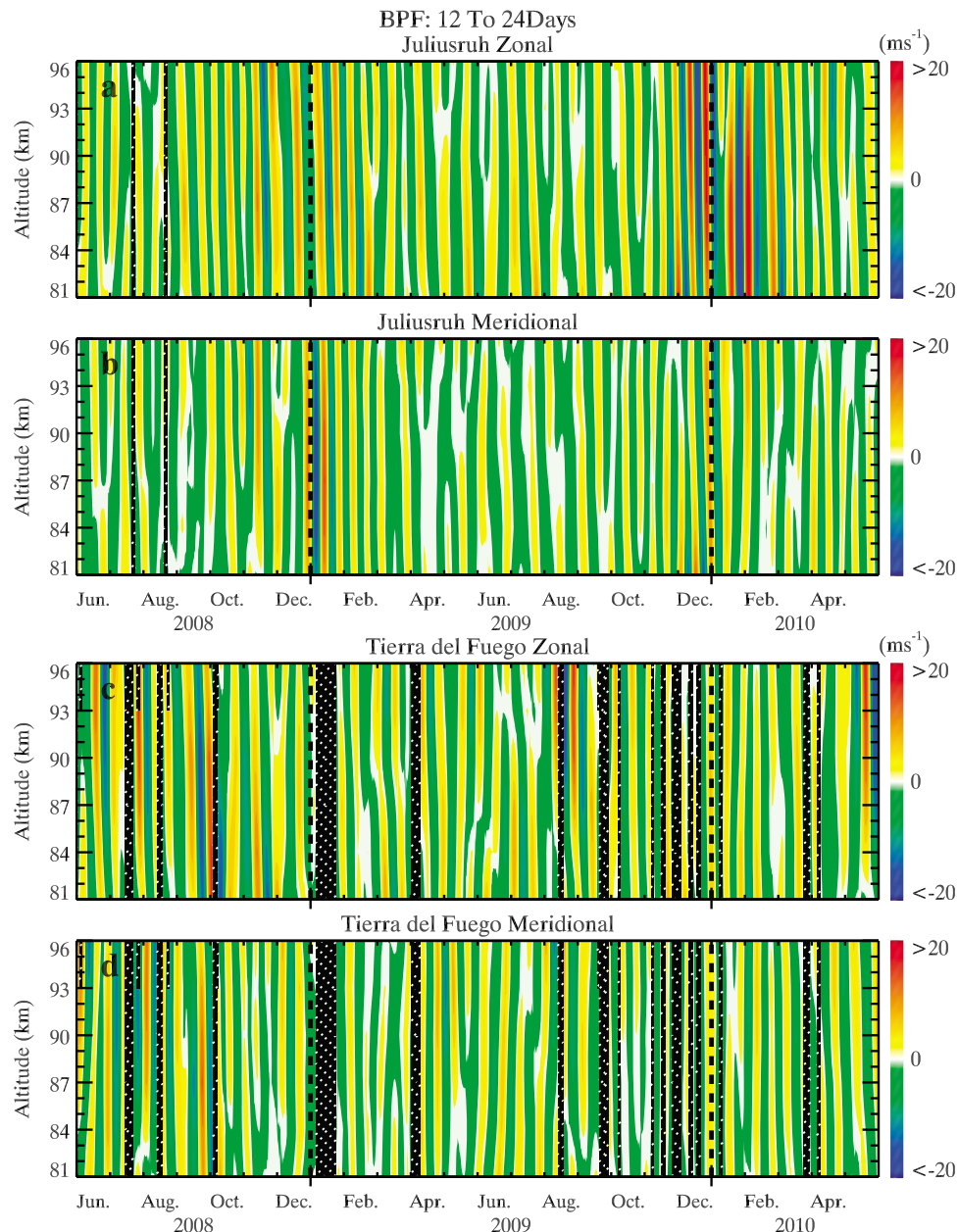


Figure 7. As in Figure 5 but for 12–24 day band pass winds.

zonal amplitudes by ~ 20 – 30 days until the maximum amplitudes in January 2009 are approached. Phase structures exhibit downward progression (upward propagation) with a vertical wavelength of ~ 60 km in both components during the development of this event. The vertical wavelength increases more strongly in the zonal than in the meridional component as the maximum amplitudes are achieved. The zonal and meridional components are nearly in phase during the initial growth of this response, but phases are more nearly in quadrature as the peak response is attained in January (see Figure 6, top). At this time, the wind vector rotates counter-clockwise with time and altitude.

[28] The major ~ 10 day PW response during the second year exhibits an earlier development in both components, a minimum in the zonal response near the beginning of 2010, and a resurgence to the largest ~ 10 day PW amplitude seen

over JLR during January and February 2010 (exceeding 20 ms^{-1} at the lowest altitudes in early February). The zonal phase is nearly constant with altitude at early stages, has a vertical wavelength approaching ~ 60 km during strong amplitude growth (as seen in the strong meridional component in the first event) and thereafter. Meridional phase variations remain nearly uniform in altitude throughout this event. However, a near quadrature relation between components is seen at the highest rather than the lowest altitudes, and a more nearly in-phase relation occurs at lower altitudes and later times (see Figure 6).

[29] In contrast to the ~ 10 day PW responses over JLR, those over TdF are more diffuse, less consistent between the zonal and meridional components, and more variable throughout the annual cycle and in the PW period (see Figures 5c, 5d, 6e, and 6f). Maximum amplitudes of

$\sim 10\text{--}15\text{ ms}^{-1}$ occur in the zonal component at higher altitudes in June and July and from late September into October 2008, at lower altitudes during November and December 2008, briefly in July 2009, and in February and April 2010. Among the stronger events, meridional amplitudes are smaller in most cases, but are comparable to, or exceed, zonal amplitudes in July and August 2008, February and March 2009, and April 2010. Surprisingly, the largest zonal amplitudes from October to December 2008 ($\sim 15\text{ ms}^{-1}$) coincide with meridional amplitudes $\sim 3\text{--}5$ times smaller. A similar amplitude disparity is seen during February 2010 at lower altitudes. Where amplitudes are well defined, phase variations are largely consistent with those noted in the discussion of responses over JLR (especially in early 2010); these are more nearly in-phase (antiphase) over JLR (TdF), respectively (see, e.g., June, July, and October 2008 at higher altitudes and February and April 2010).

4.2.2. The $\sim 16\text{--}20$ Day PWs

[30] Amplitude and phase structures for PWs having periods of $\sim 16\text{--}20$ days defined using a 12–24 day band pass are shown as time series at specific altitudes in Figures 6c, 6d, and 6f and as contour plots in Figure 7. These results exhibit similar seasonal variability to that seen for $\sim 8\text{--}10$ day PWs, with the major responses over JLR largely confined to fall and winter seasons. In contrast, those over TdF are more widely distributed throughout each year. The 12–24 day band pass results exhibit greater apparent variability of the PW periods than seen in the 7–12 day band pass, however. Two factors that likely contribute to this variability in observed PW periods in the $\sim 12\text{--}24$ day band pass include (1) their slower phase speeds and greater potential for Doppler shifting by spatially and/or temporally varying mean and quasi-stationary PW winds and (2) the possible presence of additional traveling PWs, depending on the propagation environment [see *Forbes*, 1995, Figure 3].

[31] The first interval showing enhanced $\sim 16\text{--}20$ day amplitudes over JLR extends from \sim October 2008 to February 2009 (see Figure 6c and Figures 7a and 7b). Given the observed variability in amplitude and phase structures (as seen in the 7–12 day band pass winds over JLR during this time), these fields likely represent several successive or superposed responses in reality. Zonal and meridional winds at higher altitudes are nearly in phase as amplitudes increase in October and November and suggest a period of $\sim 12\text{--}15$ days. In December, however, the wind components suggest a longer period in the zonal component, a superposition of longer and shorter periods in the meridional component, and an evolution toward a more nearly antiphase relation. Longer-period motions persist in the zonal component throughout January, yielding a nearly in-phase relation in mid February 2009. Both components exhibit phase descent with time, except for the meridional component in late December and early January, where phases appear nearly constant in altitude. The more gradual descent of phase slopes seen in the zonal wind during January suggests a vertical wavelength of ~ 40 km.

[32] The second interval exhibiting significant $\sim 16\text{--}20$ day amplitudes over JLR extends from \sim November 2009 to February 2010. As seen in the first interval, there is evidence of a possible superposition of modes, given the lack of uniformity of the phase structures with time and between the two wind components. Initial amplitude growth appears

to occur first at lower altitudes; however, the largest amplitudes occur in the zonal winds at higher altitudes during December and at lower and middle altitudes in January and February (each exceeding 20 ms^{-1}). Phase variations exhibit downward progression (suggesting upward propagation) during December (with initial vertical wavelengths of ~ 60 km), but become more nearly constant with altitude by late January. Variations of phase with altitude and time also imply varying phase relations between the wind components. The early evolution of the second event exhibits a nearly quadrature relation between zonal and meridional winds during November and December 2009 at lower altitudes; however, a more nearly in-phase relation occurs at higher altitudes as the maximum amplitudes are achieved. Apparent superpositions thereafter yield more jumbled phase structures exhibiting little coherence in altitude or time, except for the strong ~ 15 day response from mid January to mid February.

[33] Amplitudes and phases of the $\sim 16\text{--}20$ day PWs over TdF are shown with contour plots in Figure 7c and 7d and at specific altitudes in Figure 6f. As seen over JLR, the largest responses occur primarily during fall at lower altitudes and winter at higher altitudes (\sim April through September), but also extend into spring (October and November). Unlike JLR, significant amplitudes are also observed during summer, consistent with the behavior noted for the $\sim 8\text{--}10$ day amplitudes observed over TdF. In contrast with the $\sim 16\text{--}20$ day PWs seen over JLR, but consistent with the $\sim 8\text{--}10$ day PWs seen over TdF, the $\sim 16\text{--}20$ day PWs seen over TdF during both fall/winter seasons exhibit a largely antiphase relation between the wind components wherever larger amplitudes are observed, except in June 2008. This occurs despite the apparently more temporally variable PW amplitudes, periods, and phase structures over TdF at these times. This variability suggests more significant PW superpositions within this band pass than over JLR during the comparable northern hemisphere seasons. Given this, it is even more surprising that the phases of the zonal and meridional components are so highly anticorrelated during these times.

4.2.3. Wind Hodographs

[34] Hodographs of the monthly 7–12 day band-passed winds at 81 and 96 km are shown in Figure 8 for the fall and winter seasons over JLR and TdF. As noted above, maximum responses are seen over JLR during December, January, and February in each season. The $\sim 8\text{--}10$ day vector winds are seen to remain small in December 2008, but to increase with time at both altitudes during January 2009 and with the same counterclockwise rotation and approximate quadrature between components at the two altitudes. The major axis of the velocity field later in January at both altitudes is approximately NNE–SSW. Vector winds decay during February and have the same sense of rotation and phase variation in altitude seen in January. But they now have an orbital ellipse with a major axis aligned NE–SW, indicating more nearly comparable amplitudes in the two components accompanying amplitude decay.

[35] The $\sim 8\text{--}10$ day vector winds over JLR during December 2009 exhibit large amplitudes (and counterclockwise rotation) early in the month, decay thereafter, and appear to be largely unconnected to the larger responses that follow. An apparently separate event emerging in January exhibits significant amplitude growth throughout the month and a counterclockwise rotation of the wind vector at 96 km,

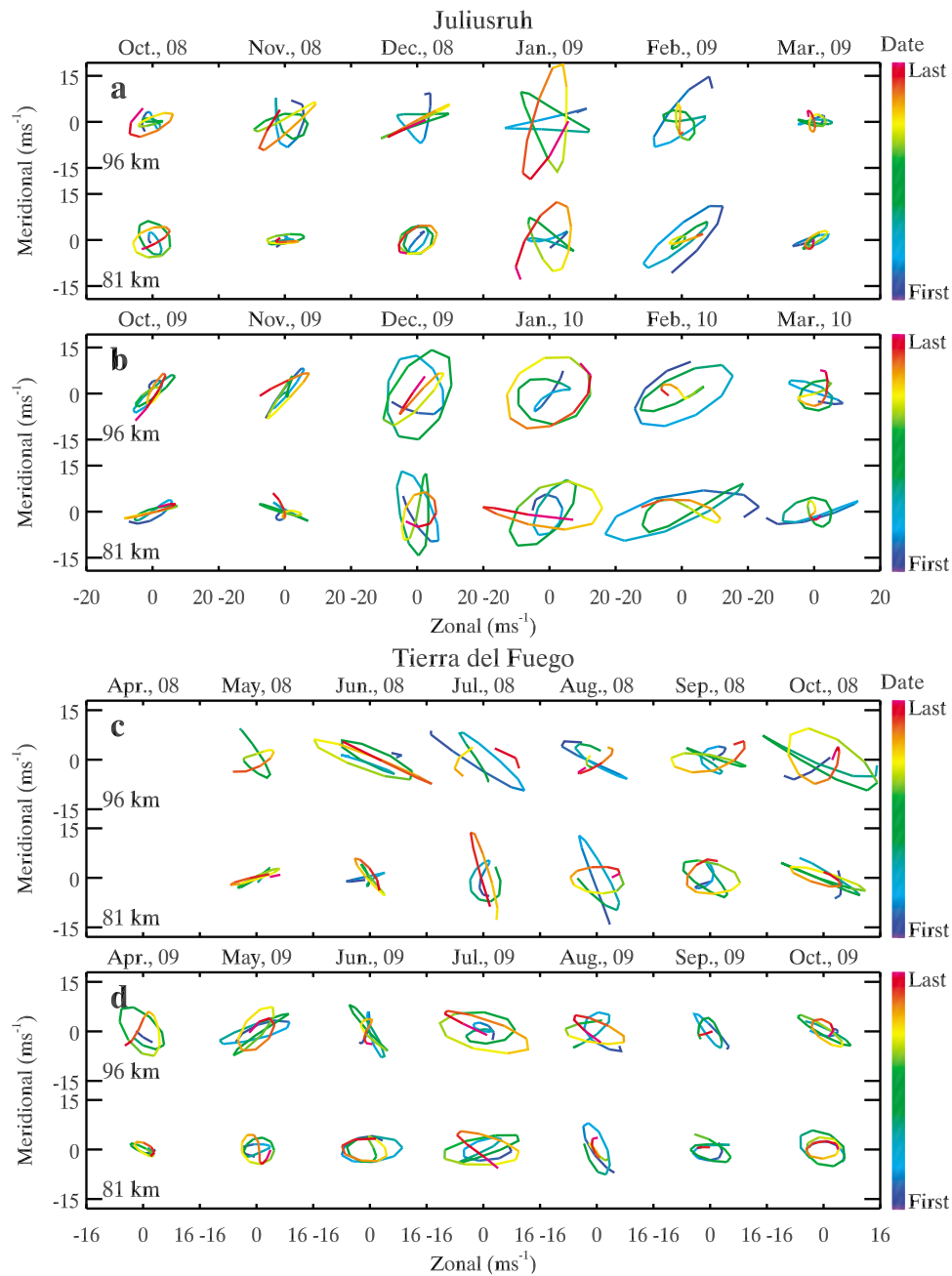


Figure 8. Hodographs of monthly 7–12 day band pass winds over (a and b) JLR and (c and d) TdF. Intervals are October 2008 to March 2009 (Figure 8a), October 2009 to March 2010 (Figure 8b), April to October 2008 (Figure 8c), and April to October 2009 (Figure 8d). Blue (red) indicates the first (last) day in each month.

but a clockwise rotation of the wind vector at 81 km that appears to reverse near the end of the month. This event exhibits a decay in February, a counterclockwise rotation while amplitudes are large, and an increased in-phase relation among components as seen in early 2008. Thus, there are significant similarities between the major ~ 8 – 10 day PW events during fall and winter seasons over JLR during the two seasons observed.

[36] Referring now to the ~ 8 – 10 day responses over TdF shown in Figures 8c and 8d, we note a very different PW morphology throughout austral fall and winter. While there

are individual months that exhibit winds comparable to those seen over JLR, there are no consistent seasonal maxima during the intervals displayed. Significant winds (approaching $\sim 20 \text{ ms}^{-1}$) occur primarily at the higher altitudes during June, July, and October 2008. Weaker winds occur at lower altitudes and other times, including the months displayed for 2009. There are, nevertheless, common features in the responses over JLR and TdF. The tendencies for correlations between the wind components appear generally antisymmetric about the equator, with largely positive correlations at northern latitudes and negative correlations at southern

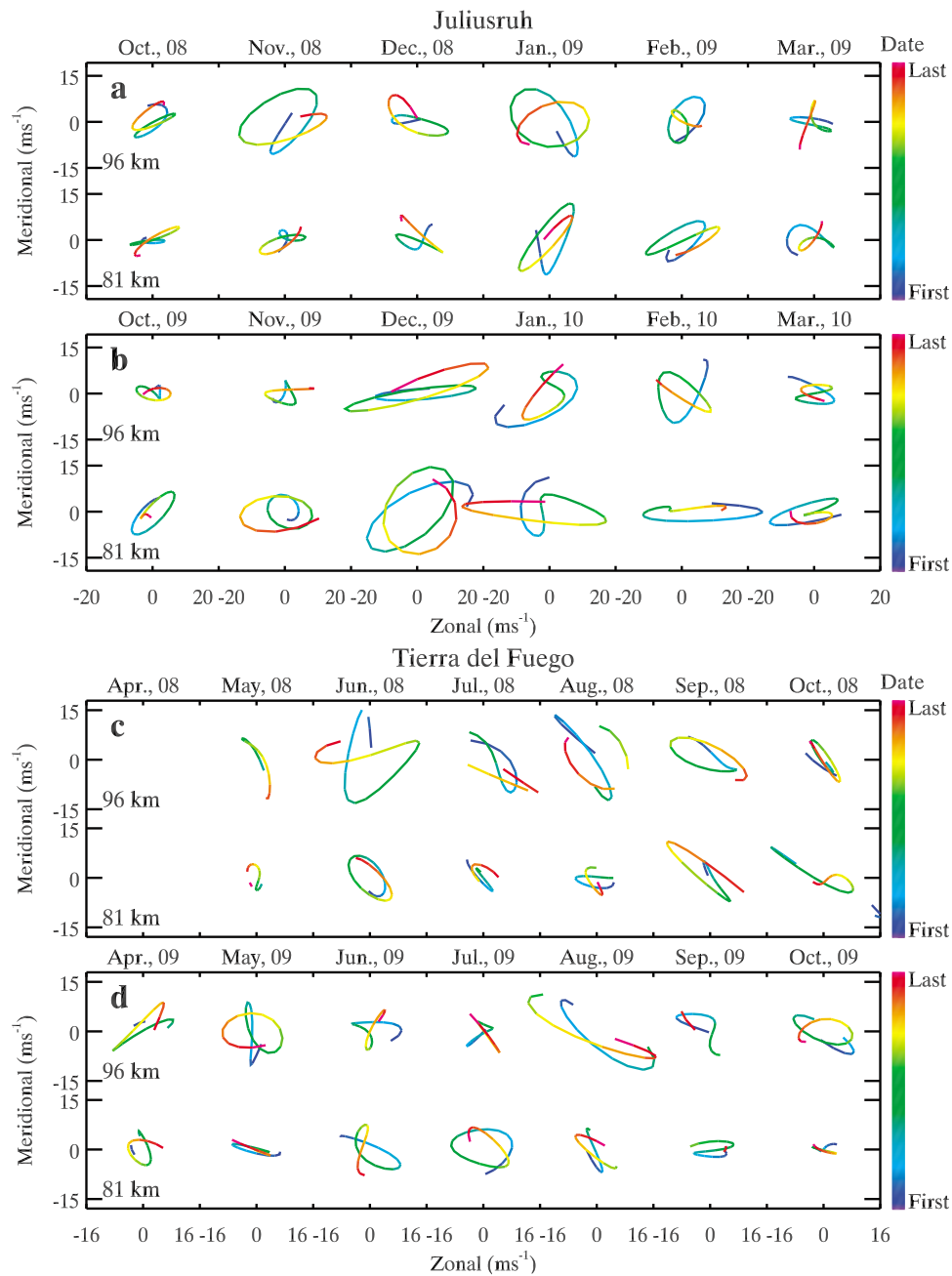


Figure 9. As in Figure 8 but for monthly 12–24 day band pass winds.

latitudes. These tendencies also exhibit some consistency in altitude and time. In terms of consistent seasonal variations in PW amplitudes, however, the 7–12 day band pass responses have very little in common between JLR and TdF.

[37] Hodographs of the monthly 12–24 day band-pass winds at 81 and 96 km are shown in Figure 9 for the fall and winter seasons over JLR and TdF. As noted in the discussion of Figures 5–7 and seen for the 7–12 day band-pass hodographs above, distinct maxima over JLR occur from ~November to February each year. In most cases, there is a clear counterclockwise rotation of the wind vector, except where evidence of PW superposition is observed. There is also a weak tendency for positive correlations between zonal

and meridional winds during the growth phases of these events; less distinct correlations are seen during the decay phases.

[38] As seen for the 7–12 day band pass hodographs, those for the 12–24 day band pass in Figure 9 reveal a very different PW morphology over TdF in austral fall and winter than seen over JLR. While there are individual months that exhibit winds comparable to those seen over JLR, maxima appear to occur during late fall and winter, and there is a tendency for negative correlations between zonal and meridional winds (and an antisymmetric response about the equator), there is also significantly greater amplitude and phase variability with altitude and time over TdF than seen

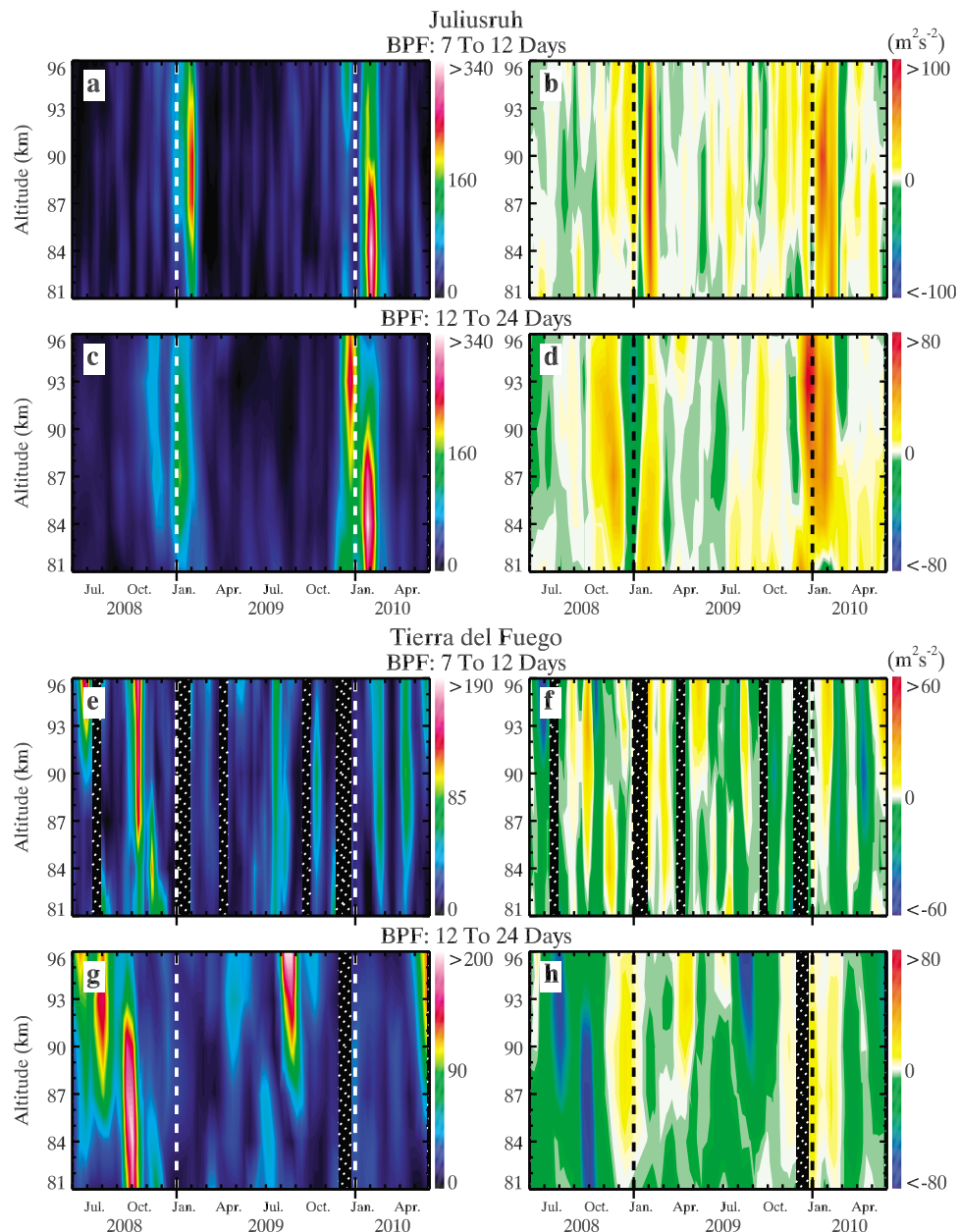


Figure 10. Horizontal wind variances as functions of time and altitude for band passes of (a and e) 7–12 days and (c and g) 12–24 days over JLR (Figure 10a and 10c) and TdF (Figure 10e and 10g). (b, d, f, and h) Same as in Figures 10a, 10c, 10e, and 10g but for horizontal momentum fluxes $\langle u'v' \rangle$. Hatched regions are as in Figure 1.

over JLR. This suggests a more complex superposition of PWs at southern than northern latitudes during fall and winter seasons.

4.2.4. Horizontal Velocity Variances

[39] Horizontal velocity variances in the 7–12 day and 12–24 day PW band passes are shown over JLR in Figures 10a and 10c and over TdF in Figures 10e and 10g. These illustrate much more clearly than the S transforms and band pass winds the temporal and altitude localization of PW activity within each band pass. The upper panels reveal that PW activity is highly localized from \sim November to February each year over JLR, and that significant variances in the 12–24 day band pass typically precede or accompany enhanced

variances in the 7–12 day band pass and are also coincident in altitude. Surprisingly, the variances in the two bands also have comparable magnitudes during the dominant responses in January and February 2010, $\sim 300 \text{ m}^2 \text{ s}^{-2}$, suggesting peak 30 day mean RMS amplitudes of $\sim 12 \text{ ms}^{-1}$ assuming comparable amplitudes in both components.

[40] PW activity over TdF is more broadly distributed throughout the year, but with primary maxima typically occurring during fall and winter. Maximum variances over TdF are $\sim 200 \text{ m}^2 \text{ s}^{-2}$ in the 12–24 day band pass and $\sim 20\%$ smaller in the 7–12 day band pass. Unlike the PW fields over JLR, the variances in the two band passes over TdF exhibit few obvious correlations, though the maxima in the

two band passes occurring in mid to late June 2008 at higher altitudes could indicate a link. In this case, the 12–24 day band pass response precedes the 7–12 day band pass response, as seen over JLR. A similar link is suggested between the 12–24 day band pass variance maximum during September and October 2008 and the successive 7–12 day band pass variance maximum in early October 2008 at somewhat higher altitudes.

4.2.5. Horizontal Momentum Fluxes

[41] Horizontal momentum fluxes implied by the correlations between wind components seen in the hodographs discussed above are shown continuously in time and altitude in Figure 10 (right) in the same format as the band pass variances at left for easy reference. Comparing these panels, we see immediately that the variance maxima seen in both band passes over JLR coincide closely with positive momentum flux maxima.

[42] Identical arguments about the correlations between PW variances and momentum fluxes over TdF can be made by examination of the corresponding variances and momentum fluxes shown in the two PW bands in Figures 10e–10h. In this case, however, the most conspicuous negative momentum flux maxima seen in Figure 10h correlate strongly with the variance maxima in each PW band pass seen in Figure 10g. As seen over JLR, mean momentum fluxes over TdF from midspring through midsummer are weakly positive and of the opposite sign to the strong fall and winter responses.

5. Discussion

[43] As seen above, mean eastward and westward winds over JLR and TdF in winter and summer are comparable at lower altitudes. Peak magnitudes are $\sim 20\text{--}30\text{ ms}^{-1}$ and slightly larger over TdF, apart from the anomalous peak over JLR in February 2009 following the largest stratospheric warming on record. At higher altitudes, monthly mean winds are predominantly eastward over JLR and entirely eastward over TdF. Summer maxima are more distinct over JLR and magnitudes are $\sim 30\text{ ms}^{-1}$ or greater over both sites. Comparing these mean winds with those measured over Andenes (69°N) and Syowa (69°S) by *Imura et al.* [2011] from 1999 to 2010, we see that summer westward winds are comparable at the northern latitudes and stronger at the higher southern latitude, but that winter eastward winds are significantly weaker at the higher latitudes in each hemisphere.

[44] Mean equatorward winds in summer were seen in our discussion in section 3 to be stronger over JLR ($>10\text{ ms}^{-1}$) than over TdF at lower altitudes, but to be centered at somewhat higher altitudes over TdF. Mean meridional winds in winter, in contrast, are weak and poleward in the seasonal means at JLR and TdF, but highly variable in the monthly means. Comparing these results with those of *Imura et al.* [2011], we see that the equatorward summer winds over JLR are larger than over Andenes, but that this latitudinal gradient is reversed at southern latitudes, with equatorward winds somewhat larger over Syowa than over TdF, but also much more confined in altitude. Mean meridional winds in winter at higher latitudes (Andenes and Syowa) are likewise weak in both hemispheres. But both also exhibit a reversal from mean poleward motions at lower altitudes to mean

equatorward motions at higher altitudes, in sharp contrast with the winds over JLR and TdF.

[45] PW results presented above are generally consistent with previous studies of the “10 day” and “16 day” waves at middle and high latitudes. Large PW amplitudes are largely confined to fall and winter seasons, but smaller amplitude responses occur throughout the year over both JLR and TdF. Large amplitudes in both bands are also more narrowly confined to late fall and early winter over JLR than over TdF, and more so in the meridional than in the zonal winds at both sites. The former appears to differ from the 16 day wave results of *Day and Mitchell* [2010b] for Rothera and Esrange at somewhat higher latitudes, but may be a further indication of the significant interannual variability noted in both studies. The latter is consistent with the occurrence statistics reported by *Murphy et al.* [2007] for their 8–16 day band pass results over Davis, Antarctica. Maximum amplitudes of the ~ 16 day wave in our 12–24 day band pass exceed 20 ms^{-1} at both JLR and TdF, and are thus somewhat larger than seen by *Day and Mitchell* [2010b] over Esrange (68°N) and Rothera (68°S) and by *Murphy et al.* [2007] over Davis (69°S).

[46] The largest PW amplitudes in our study are seen over JLR, though they do not occur every year. Our maximum amplitudes are $\sim 100\%$ larger than observed at comparable northern latitudes by *Mitchell et al.* [1999] over Sheffield (54°N), by *Forbes et al.* [1995] over Obninsk (54°N) and Saskatoon (52°N), and by *Luo et al.* [2002] at multiple locations. Maximum amplitudes of the ~ 10 day wave are $\sim 20\text{--}50\%$ smaller than those of the ~ 16 day wave. These differences may not be significant, however, given the different radars and band pass methods employed for these various studies. Maximum amplitudes of the ~ 10 day wave in our study also exceed 20 ms^{-1} , but are typically somewhat smaller than for the ~ 16 day wave. Similar tendencies for larger 16 day PW amplitudes in winter and in the northern hemisphere were also observed in the analysis of Microwave Limb Sounder temperatures from August 2004 to June 2010 by *Day et al.* [2010].

[47] Where PW amplitudes are large and the rotation of the wind vector is well defined, the predominant sense of rotation is counterclockwise over JLR. This is consistent with that seen for the 16 day PW over Sheffield by *Mitchell et al.* [1999]. Orbital ellipses are less well defined, in general, over TdF, and may be an indication of more significant PW superpositions or interactions at southern latitudes.

[48] The temporal behavior of the significant PW responses in the S transforms displayed in Figure 3 suggests somewhat different morphologies of, and/or nonlinear interactions involving, the PWs in each hemisphere. Strong isolated responses occur from \sim November to February each year over JLR, each including simultaneous responses at different periods or events that appear to arise having one period, but quickly evolve to another. Such coupled responses may be an indication of common or evolving sources of the various PW responses. We also note, however, that more complex coupling among different components of the motion field may be suggested by smaller-amplitude motions over JLR, as discussed further below. S transforms for TdF, in contrast, exhibit multiple maxima that often appear to evolve through more complex interactions among PWs having several periods, though at smaller amplitudes than

the dominant responses over JLR. Indeed, these apparent links among different responses in the S transforms appear very similar to those seen in the spectrograms shown by Mitchell *et al.* [1999] over Sheffield. Additional evidence of possible PW interactions is provided by the lack of spatial coherence of the 16 day wavefields observed simultaneously at multiple Northern Hemisphere locations by Luo *et al.* [2002]. Thus, while the dominant responses appear to have somewhat different character in the two hemispheres, the underlying dynamics at smaller amplitudes appear to be a common feature of both.

[49] To the extent that large momentum fluxes are indicative of significant PW-mean flow interactions, these results may provide clues to the character of these interactions and the potential for barotropic and/or baroclinic instabilities of the mean flow as the source of the observed PWs. Zonal mean winds in the Global Empirical Wind Model (GEWM) indicate curvature of the zonal wind on the poleward flanks of the wintertime midlatitude jet [Portnyagin *et al.*, 2004]. At JLR, positive momentum fluxes in the wintertime months are consistent with the typical SW-NE alignment of large scale, amplifying perturbations. Thus, the PW variances, fluxes, and climatological mean winds at JLR fit into a model of barotropic instability. Likewise, the strong negative momentum fluxes during late winter at TdF, and the climatological wind pattern, are consistent with a southern hemisphere version of the instability. Momentum flux estimates at single sites are not sufficient to fully diagnose PW-mean flow interactions, however. This requires definition of the mean wind and temperature fields and a more complete characterization of the various contributions to the Eliassen-Palm flux as functions of latitude and time than can be accomplished with discrete wind measurements. We also note that our negative momentum fluxes over TdF are of the same sign as the mean over Davis during Austral winter [Murphy *et al.*, 2007], but that the mean positive momentum fluxes seen over Davis from September through December occur ~ 2 months earlier relative to our more limited observations.

6. Summary and Conclusions

[50] We employed meteor radars at approximately conjugate latitudes (Juliusruh, Germany, 54.6°N , and Rio Grande, Argentina, 53.8°S) for interhemispheric comparisons of mean winds and planetary wave structures from June 2008 to May 2010 for which coincident and nearly continuous data were available.

[51] Differences in mean winds between the two sites include the following: (1) westward monthly mean winds extending to higher altitudes over JLR than over TdF during early spring each year; (2) significantly stronger westward monthly mean winds from ~ 81 – 90 km over TdF during late spring 2008 than seen over JLR either year; (3) comparable or larger eastward monthly mean winds during fall and winter (greater by ~ 5 – 20 ms^{-1}) over TdF than over JLR, except for an anomalously strong eastward monthly mean wind over JLR in February 2009 accompanying the strongest and most prolonged stratospheric warming on record [Manney *et al.*, 2009]; (4) equatorward monthly mean winds during late spring and early summer at each site that achieve amplitudes of ~ 5 – 10 ms^{-1} at lower altitudes, slightly larger amplitudes over JLR, and amplitudes that decay more slowly

at higher altitudes over TdF; and (5) meridional mean winds during fall and winter that are weakly poleward (except during the January 2009 stratospheric warming) and more variable than during spring and summer because they are significantly impacted by PW and lower-frequency oscillations.

[52] Both JLR and TdF exhibit PW and longer-period oscillations extending from ~ 8 – 40 days. Shorter-period PWs were specifically excluded from this analysis and will be examined separately. Dominant PW responses occur at periods of ~ 8 – 10 and 16 – 20 days over both sites, with these motions more strongly confined to late fall and early winter months over JLR than over TdF. These responses are more nearly coincident over JLR and more typically sequential over TdF, suggesting different source and/or interaction dynamics in the two hemispheres. Horizontal momentum fluxes evaluated by the two radars are typically strongly positive (negative) over JLR (TdF) during large PW responses, suggestive of sources due to barotropic instability. However, these radar wind measurements by themselves are insufficient to diagnose the potential PW-mean flow dynamics fully, and an expanded study employing satellite data is envisioned for this purpose.

[53] To investigate the possible indications of PW-mean flow interactions further, the behavior at JLR and TdF must be placed into a global-scale context. Satellite winds from TIMED, and temperatures from TIMED or EOS/MLS, will be used to define the PW fields at these and other latitudes in a follow-on to the present study. The global extent of these data will enable calculation of meridional gradients of PW momentum fluxes, and their effects on the mean flow. Satellite data will also allow the role of heat fluxes to be examined.

[54] **Acknowledgments.** Research described here was performed under NSF grant ATM-0634650. The authors are very grateful for the valuable support of personnel at Estacion Astronomica Rio Grande (EARG) for their assistance with the operations and maintenance of SAAMER. We also thank Chris Hall and two anonymous reviewers for very valuable comments on the manuscript.

References

- Andrews, D. G. (1989), Some comparisons between the middle atmosphere dynamics of the southern and northern hemispheres, *Pure Appl. Geophys.*, *130*, 213–232, doi:10.1007/BF00874456.
- Avery, S. K., R. A. Vincent, A. Phillips, A. H. Manson, and G. J. Fraser (1989), High-latitude tidal behavior in the mesosphere and lower thermosphere, *J. Atmos. Terr. Phys.*, *51*, 595–608, doi:10.1016/0021-9169(89)90057-3.
- Bailey, S. M., A. W. Merkel, G. E. Thomas, and D. W. Rusch (2007), Hemispheric differences in polar mesospheric cloud morphology observed by the student nitric oxide explorer, *J. Atmos. Sol. Terr. Phys.*, *69*, 1407–1418.
- Burrage, M. D., D. L. Wu, W. R. Skinner, D. A. Ortland, and P. B. Hays (1995), Latitude and seasonal dependence of the semidiurnal tide observed by the high-resolution Doppler imager, *J. Geophys. Res.*, *100*, 11,313–11,321, doi:10.1029/95JD00696.
- Charney, J. G., and D. M. Straus (1980), Form-drag instability, multiple equilibria and propagating planetary waves in baroclinic, orographically forced, planetary wave systems, *J. Atmos. Sci.*, *37*, 1157–1176, doi:10.1175/1520-0469(1980)037<1157:FDIMEA>2.0.CO;2.
- Chu, X., C. S. Gardner, and R. G. Roble (2003), Lidar studies of interannual, seasonal, and diurnal variations of polar mesospheric clouds at the South Pole, *J. Geophys. Res.*, *108*(D8), 8447, doi:10.1029/2002JD002524.
- Day, K. A., and N. J. Mitchell (2010a), The 5-day wave in the Arctic and Antarctic mesosphere and lower thermosphere, *J. Geophys. Res.*, *115*, D01109, doi:10.1029/2009JD012545.

- Day, K. A., and N. J. Mitchell (2010b), The 16-day wave in the Arctic and Antarctic mesosphere and lower thermosphere, *Atmos. Chem. Phys.*, *10*, 1461–1472, doi:10.5194/acp-10-1461-2010.
- Day, K. A., R. E. Hibbins, and N. J. Mitchell (2010), Aura MLS observations of the westward-propagating $s = 1$, 16-day planetary wave in the middle atmosphere: Climatology and cross-equatorial propagation, *Atmos. Chem. Phys. Discuss.*, *10*, 23,197–23,227, doi:10.5194/acpd-10-23197-2010.
- Dowdy, A., R. A. Vincent, K. Igarashi, Y. Murayama, and D. J. Murphy (2001), A comparison of mean winds and gravity wave activity in the northern and southern polar MLT, *Geophys. Res. Lett.*, *28*, 1475–1478, doi:10.1029/2000GL012576.
- Dowdy, A. J., R. A. Vincent, M. Tsutsumi, K. Igarashi, Y. Murayama, W. Singer, and D. J. Murphy (2007), Polar mesosphere and lower thermosphere dynamics: 1. Mean wind and gravity wave climatologies, *J. Geophys. Res.*, *112*, D17104, doi:10.1029/2006JD008126.
- Eckermann, S. D., D. K. Rajopadhyaya, and R. A. Vincent (1997), Intra-seasonal wind variability in the equatorial mesosphere and lower thermosphere: Long-term observations from the central Pacific, *J. Atmos. Sol. Terr. Phys.*, *59*, 603–627, doi:10.1016/S1364-6826(96)00143-5.
- Farrell, B. (1988), Optimal excitation of neutral Rossby waves, *J. Atmos. Sci.*, *45*, 163–172, doi:10.1175/1520-0469(1988)045<0163:OEONRW>2.0.CO;2.
- Farrell, B. F., and P. J. Ioannou (1996), Generalized stability theory. Part I: Autonomous operators, *J. Atmos. Sci.*, *53*, 2025–2040, doi:10.1175/1520-0469(1996)053<2025:GSTPIA>2.0.CO;2.
- Forbes, J. M. (1995), Tidal and planetary waves, in *The Upper Mesosphere and Lower Thermosphere: A Review of Experiment and Theory*, *Geophys. Monogr. Ser.*, vol. 87 edited by R. M. Johnson and T. L. Killeen, pp. 67–87, AGU, Washington, D. C., doi:10.1029/GM087p0067.
- Forbes, J. M., M. E. Hagan, S. Miyahara, F. Vial, A. H. Manson, C. E. Meek, and Y. Portnyagin (1995), Quasi 16-day oscillation in the mesosphere and lower thermosphere, *J. Geophys. Res.*, *100*, 9149–9163, doi:10.1029/94JD02157.
- Fraser, G. J., Y. I. Portnyagin, J. M. Forbes, R. A. Vincent, I. A. Lysenko, and N. A. Makarov (1995), Diurnal tide in the Antarctic and Arctic mesosphere/lower thermosphere regions, *J. Atmos. Terr. Phys.*, *57*, 383–393, doi:10.1016/0021-9169(94)E0010-K.
- Fritts, D. C., D. Janches, H. Iimura, W. K. Hocking, N. J. Mitchell, B. Fuller, B. Vandepuer, J. Hormaechea, C. Brunini, and H. Levato (2010a), Southern Argentina agile meteor radar: System design and initial measurements of large-scale winds and tides, *J. Geophys. Res.*, *115*, D18112, doi:10.1029/2010JD013850.
- Fritts, D. C., D. Janches, and W. K. Hocking (2010b), Southern Argentina agile meteor radar (SAAMER): Initial assessment of gravity wave momentum fluxes, *J. Geophys. Res.*, *115*, D19123, doi:10.1029/2010JD013891.
- Hervig, M., and D. Siskind (2006), Decadal and inter-hemispheric variability in polar mesospheric clouds, water vapor, and temperature, *J. Atmos. Sol. Terr. Phys.*, *68*, 30–41.
- Hirooka, T., and I. Hirota (1985), Normal mode Rossby waves observed in the upper stratosphere. Part II: Second antisymmetric and symmetric modes of zonal wavenumbers 1 and 2, *J. Atmos. Sci.*, *42*, 536–548, doi:10.1175/1520-0469(1985)042<0536:NMRWOI>2.0.CO;2.
- Huaman, M. M., and B. B. Balsley (1999), Differences in near-mesopause summer winds, temperatures, and water vapor at northern and southern latitudes as possible causal factors for inter-hemispheric PMSE differences, *Geophys. Res. Lett.*, *26*, 1529–1532, doi:10.1029/1999GL00294.
- Huang, F. T., H. G. Mayr, C. A. Reber, J. Russell, M. Mlynczak, and J. Mengel (2006), Zonal-mean temperature variations inferred from SABER measurements on TIMED compared with UARS observations, *J. Geophys. Res.*, *111*, A10S07, doi:10.1029/2005JA011427.
- Iimura, H., D. C. Fritts, Q. Wu, W. R. Skinner, and S. D. E. Palo (2010), Nonmigrating semidiurnal tide over the Arctic determined from TIMED Doppler Interferometer wind observations, *J. Geophys. Res.*, *115*, D06109, doi:10.1029/2009JD012733.
- Iimura, H., D. C. Fritts, M. Tsutsumi, T. Nakamura, P. Hoffman, and W. Singer (2011), Long-term observations of the wind fields in the Arctic and Antarctic mesosphere and lower thermosphere at conjugate latitudes, *J. Geophys. Res.*, *116*, D20112, doi:10.1029/2011JD016003.
- Isoda, F., T. Tsuda, T. Nakamura, Y. Murayama, K. Igarashi, R. A. Vincent, I. M. Reed, A. Nuryanto, and S. L. Manurung (2002), Long-period wind oscillations in the mesosphere and lower thermosphere at Yamagawa (32°N, 131°E), Pontianak (0°N, 109°E) and Christmas Island (2°N, 157°W), *J. Atmos. Sol. Terr. Phys.*, *64*, 1055–1067, doi:10.1016/S1364-6826(02)00057-3.
- Kishore, P., S. P. Namboothiri, K. Igarashi, Y. Murayama, R. A. Vincent, A. Dowdy, D. J. Murphy, and B. J. Watkins (2003), Further evidence of hemispheric differences in the MLT mean wind climatology: Simultaneous MF radar observations at Poker Flat (65°N, 147°W) and Davis (69°S, 78°E), *Geophys. Res. Lett.*, *30*(6), 1336, doi:10.1029/2002GL016750.
- Luo, Y., A. H. Manson, C. E. Meek, K. Igarashi, and C. Jacobi (2001), Extra long period (20–40 day) oscillations in the mesospheric and lower thermospheric winds: Observations in Canada, Europe and Japan, and considerations of possible solar influences, *J. Atmos. Sol. Terr. Phys.*, *63*, 835–852, doi:10.1016/S1364-6826(00)00206-6.
- Luo, Y., et al. (2002), The 16-day planetary waves: Multi-MF radar observations from the arctic to the equator and comparisons with the HRDI measurements and the GSWM modelling results, *Ann. Geophys.*, *20*, 691–709, doi:10.5194/angeo-20-691-2002.
- Madden, R. A., and P. R. Julian (1994), Observations of the 40–50-day tropical oscillation—A review, *Mon. Weather Rev.*, *122*, 814–837, doi:10.1175/1520-0493(1994)122<0814:OOTDIO>2.0.CO;2.
- Manney, G. L., M. J. Schwartz, K. Krüger, M. L. Santee, S. Pawson, J. N. Lee, W. H. Daffer, R. A. Fuller, and N. J. Livesey (2009), Aura microwave limb sounder observations of dynamics and transport during the record-breaking 2009 Arctic stratospheric major warming, *Geophys. Res. Lett.*, *36*, L12815, doi:10.1029/2009GL038586.
- Mitchell, N. J., H. R. Middleton, A. G. Beard, P. J. S. Williams, and H. G. Muller (1999), The 16-day planetary wave in the mesosphere and lower thermosphere, *Ann. Geophys.*, *17*, 1447–1456, doi:10.1007/s00585-999-1447-9.
- Miyoshi, Y. (1999), Numerical simulation of the 5-day and 16-day waves in the mesopause region, *Earth Planets Space*, *51*, 763–772.
- Mukhtarov, P., D. Pancheva, and B. Andonov (2010), Climatology of the stationary planetary waves seen in the SABER/TIMED temperatures (2002–2007), *J. Geophys. Res.*, *115*, A06315, doi:10.1029/2009JA015156.
- Murphy, D. J., W. J. R. French, and R. A. Vincent (2007), Long-period planetary waves in the mesosphere and lower thermosphere above Davis, Antarctica, *J. Atmos. Sol. Terr. Phys.*, *69*, 2118–2138, doi:10.1016/j.jastp.2007.06.008.
- Oberheide, J., Q. Wu, T. L. Killeen, M. E. Hagan, and R. G. Roble (2006), Diurnal nonmigrating tides from TIMED Doppler Interferometer wind data: Monthly climatologies and seasonal variations, *J. Geophys. Res.*, *111*, A10S03, doi:10.1029/2005JA011491.
- Portnyagin, Y. I., J. M. Forbes, G. M. Fraser, R. A. Vincent, S. K. Avery, I. A. Lysenko, and N. A. Makarov (1993a), Dynamics of the Antarctic and Arctic mesosphere and lower thermosphere regions—Part I. The prevailing wind, *J. Atmos. Terr. Phys.*, *55*, 827–841, doi:10.1016/0021-9169(93)90024-S.
- Portnyagin, Y. I., J. M. Forbes, G. M. Fraser, R. A. Vincent, S. K. Avery, I. A. Lysenko, and N. A. Makarov (1993b), Dynamics of the Antarctic and Arctic mesosphere and lower thermosphere regions—Part II. The semidiurnal tide, *J. Atmos. Terr. Phys.*, *55*, 843–855, doi:10.1016/0021-9169(93)90025-T.
- Portnyagin, Y., et al. (2004), Mesosphere/lower thermosphere prevailing wind model, *Adv. Space Res.*, *34*, 1755–1762.
- Portnyagin, Y. I., E. G. Merzlyakov, T. V. Solov's'eva, and N. A. Makarov (2006), Interhemispheric distinctions in wind-regime parameters in the polar mesosphere-lower thermosphere, *Izv. Ross. Akad. Nauk, Fiz. Atmos. Okeana*, *42*, 102–114.
- Randel, W. J., D. R. Stevens, and J. L. Stanford (1987), A study of planetary waves in the southern winter troposphere and stratosphere. Part II: Life cycles, *J. Atmos. Sci.*, *44*, 936–949, doi:10.1175/1520-0469(1987)044<0936:ASOPWI>2.0.CO;2.
- Riggin, D. M., C. K. Meyer, D. C. Fritts, M. J. Jarvis, Y. Murayama, W. Singer, R. A. Vincent, and D. J. Murphy (2003), MF radar observations of seasonal variability of semidiurnal motions in the mesosphere at high northern and southern latitudes, *J. Atmos. Sol. Terr. Phys.*, *65*, 483–493, doi:10.1016/S1364-6826(02)00340-1.
- Salby, M. L. (1981a), Rossby normal modes in nonuniform background configurations. Part I: Simple fields, *J. Atmos. Sci.*, *38*, 1803–1826, doi:10.1175/1520-0469(1981)038<1803:RNMINB>2.0.CO;2.
- Salby, M. L. (1981b), Rossby normal modes in nonuniform background configurations. Part II: Equinox and solstice conditions, *J. Atmos. Sci.*, *38*, 1827–1840, doi:10.1175/1520-0469(1981)038<1827:RNMINB>2.0.CO;2.
- Simmons, A. J., B. J. Hoskins, and D. M. Burridge (1978), Stability of the semi-implicit method of time integration, *Mon. Weather Rev.*, *106*, 405–412, doi:10.1175/1520-0493(1978)106<0405:SOTSIM>2.0.CO;2.
- Singer, W., J. Bremer, W. K. Hocking, J. Weiss, R. Latteck, and M. Zecha (2003), Temperature and wind tides around the summer mesopause at middle and arctic latitudes, *Adv. Space Res.*, *31*, 2055–2060, doi:10.1016/S0273-1177(03)00228-X.
- Singer, W., J. Bremer, J. Weiß, W. K. Hocking, J. Höffner, M. Donner, and P. Espy (2004a), Meteor radar observations at middle and Arctic

- latitudes. Part 1: Mean temperatures, *J. Atmos. Sol. Terr. Phys.*, *66*, 607–616, doi:10.1016/j.jastp.2004.01.012.
- Singer, W., J. Weiß, and U. von Zahn (2004b), Diurnal and annual variations of meteor rates at the arctic circle, *Atmos. Chem. Phys.*, *4*, 1355–1363, doi:10.5194/acp-4-1355-2004.
- Singer, W., R. Latteck, P. Hoffmann, B. P. Williams, D. C. Fritts, Y. Murayama, and K. Sakanoi (2005), Tides near the Arctic summer mesopause during the MaCWAVE/MIDAS summer program, *Geophys. Res. Lett.*, *32*, L07S90, doi:10.1029/2004GL021607.
- Siskind, D. E., S. D. Eckermann, J. P. McCormack, M. J. Alexander, and J. T. Bacmeister (2003), Hemispheric differences in the temperature of the summertime stratosphere and mesosphere, *J. Geophys. Res.*, *108*(D2), 4051, doi:10.1029/2002JD002095.
- Smith, A. K. (1985), Wave transience and wave-mean flow interaction caused by the interference of stationary and traveling waves, *J. Atmos. Sci.*, *42*, 529–535, doi:10.1175/1520-0469(1985)042<0529:WTAWMF>2.0.CO;2.
- Smith, A. K. (2003), The origins of stationary planetary waves in the upper mesosphere, *J. Atmos. Sci.*, *60*, 3033–3041, doi:10.1175/1520-0469(2003)060<3033:TOOSPW>2.0.CO;2.
- Stockwell, R. G., L. Mansinha, and R. Lowe (1996), Localization of the complex spectrum: The S transform, *IEEE Trans. Signal Process.*, *44*, 998–1001, doi:10.1109/78.492555.
- Szasz, C., J. Kero, A. Pellinen-Wannberg, J. D. Matthews, N. J. Mitchell, and W. Singer (2004), Latitudinal variations of diurnal meteor rates, *Earth Moon Planets*, *95*, 101–107, doi:10.1007/s11038-005-9007-0.
- Vial, F. (1989), Tides in the middle atmosphere, *J. Atmos. Terr. Phys.*, *51*, 3–17, doi:10.1016/0021-9169(89)90069-X.
- Vincent, R. A., T. Tsuda, and S. Kato (1988), A comparative study of mesospheric solar tides observed at Adelaide and Kyoto, *J. Geophys. Res.*, *93*, 699–708, doi:10.1029/JD093iD01p00699.
- Volland, H. (1988), *Atmospheric Tidal and Planetary Waves*, 348 pp., Kluwer Acad., Boston.
- Williams, C. R., and S. K. Avery (1992), Analysis of long-period waves using the mesosphere-stratosphere-troposphere radar at Poker Flats, Alaska, *J. Geophys. Res.*, *97*, 20,855–20,861.
- Xu, J., A. K. Smith, W. Yuan, H.-L. Liu, Q. Wu, M. G. Mlynczak, and J. M. Russell III (2007a), Global structure and long-term variations of zonal mean temperature observed by TIMED/SABER, *J. Geophys. Res.*, *112*, D24106, doi:10.1029/2007JD008546.
- Xu, J., H.-L. Liu, W. Yuan, A. K. Smith, R. G. Roble, C. J. Mertens, J. M. Russell III, and M. G. Mlynczak (2007b), Mesopause structure from Thermosphere, Ionosphere, Mesosphere, Energetics, and Dynamics (TIMED)/Sounding of the Atmosphere Using Broadband Emission Radiometry (SABER) observations, *J. Geophys. Res.*, *112*, D09102, doi:10.1029/2006JD007711.

D. C. Fritts, H. Iimura, and R. Lieberman, Colorado Research Associates Division, NorthWest Research Associates, 3380 Mitchell Ln., Boulder, CO 80301, USA. (dave@cora.nwra.com)

D. Janches, Space Weather Division, NASA Goddard Space Flight Center, 8800 Greenbelt Rd., Mail Code 674, Greenbelt, MD 20771, USA.

W. Singer, Leibnitz Institute of Atmospheric Physics, Rostock University, Schloss Str. 6, Kühlungsborn D-18225, Germany.